

KIT SCIENTIFIC REPORTS 7636

MHD pressure drop at bare welding positions in pipes of DCLL blankets

Leo Bühler

Leo Bühler

MHD pressure drop at bare welding positions in pipes of DCLL blankets

Karlsruhe Institute of Technology
KIT SCIENTIFIC REPORTS 7636

MHD pressure drop at bare welding positions in pipes of DCLL blankets

by
Leo Bühler

Report-Nr. KIT-SR 7636

Impressum

Karlsruher Institut für Technologie (KIT)
KIT Scientific Publishing
Straße am Forum 2
D-76131 Karlsruhe
www.ksp.kit.edu

KIT – Universität des Landes Baden-Württemberg und
nationales Forschungszentrum in der Helmholtz-Gemeinschaft



Diese Veröffentlichung ist im Internet unter folgender Creative Commons-Lizenz
publiziert: <http://creativecommons.org/licenses/by-nc-nd/3.0/de/>

KIT Scientific Publishing 2013
Print on Demand

ISSN 1869-9669

MHD pressure drop at bare welding positions in pipes of DCLL blankets

Abstract

A systematic parametric analysis has been performed using asymptotic numerical methods for determination of MHD flows near gaps of electrically insulating inserts in well conducting pipes. Such gaps could be present at several positions in fusion blankets, where cutting and rewelding by remotely controlled tools is foreseen. Gaps in the insulation provide additional current paths which leads to increased current density and braking electromagnetic Lorentz forces. As a result the overall pressure drop increases significantly in comparison with that in a perfectly insulating pipe. The present numerical simulations suggest a simple design formula, which should give a conservative estimate of the additional pressure drop Δp_{3D} caused by induced 3D electric currents.

MHD Druckverlust an unisolierten Schweißpositionen in Rohren vom DCLL Blankets

Zusammenfassung

In dieser systematischen Parameterstudie werden mit asymptotischen numerischen Methoden MHD Strömungen an den Enden von elektrisch isolierenden Kanaleinsätzen in gut leitenden Rohren untersucht. Öffnungen zwischen Kanaleinsätzen sind an verschiedenen Stellen in Fusionsblankets nötig, an denen die Trennung und Wiederverschweißung von Rohren durch ferngesteuerte Werkzeuge vorgesehen ist. Spalten in der Isolation ermöglichen zusätzliche Strompfade, was die Gesamtstromstärke und die damit verbundenen bremsenden Lorentz-Kräfte erhöht. Dies führt zu einer beachtlichen Zunahme des Druckverlusts im Vergleich mit Strömungen in vollständig isolierten Rohren. Die durchgeführten numerischen Simulationen erlauben es, eine Druckverlustkorrelation (10) zur konservativen Abschätzung des zusätzlichen Druckverlusts Δp_{3D} anzugeben.

MHD pressure drop at bare welding positions in pipes of DCLL blankets

Contents

1	Introduction	1
2	Formulation	2
3	Results	4
3.1	Insulating inserts and walls with $c = 1.0$	4
3.2	Insulating inserts and walls with $c = 0.1$	8
3.3	Pressure drop correlation	10
3.4	Inserts with finite wall-normal conductivity	11
4	Conclusions	13
	Annex	15
	References	16

1 Introduction

Magnetohydrodynamic (MHD) pressure drops of liquid metal breeder and coolant flows in fusion blankets often exceed acceptable limits if duct walls are electrically conducting. The reason for that can be easily understood. Electric currents induced by the motion of the electrically conducting liquid alloys in the magnetic environment of a fusion reactor find a shortcut through the well-conducting walls. This yields a maximum current density in the fluid and, as a result of its interaction with the magnetic field, the electromagnetic forces generate enormous braking of the flow that has to be overcome by a corresponding high pressure head. This phenomena is known since the early days of fusion MHD research and several proposals have been made since, to reduce the pressure drop by means of insulating layers, coatings, or flow channel inserts (FCI) (see e.g. Malang, Deckers, Fischer, John, Meyder, Norajitra, Reimann, Reiser and Rust (1991)). Currently the ceramic material SiC/SiC is considered as electrical insulation material for FCIs in Dual Coolant Lead Lithium (DCLL) blankets, where the inserts serve in addition as a thermal insulation. This promising design option for power reactors allows liquid metal temperatures far beyond the wall limiting temperatures of steel with perspectives for high thermal efficiency (Norajitra, Bühler, Fischer, Kleefeldt, Malang, Reimann, Schnauder, Giancarli, Golfier, Poitevin and Salavy (2001)).

In the present work we study the influence on pressure drop of locally uninsulated regions as they may be present in DCLL blankets at positions where pipes have to be cut and re-welded when blanket modules are replaced.

As a prototypical geometry we consider a long pipe of inner radius a , wall thickness t_w and electric conductivity σ_w . Inside the pipe we have insulating inserts made of SiC/SiC with outer radius a , thickness t_i and electric conductivity σ_i . The thin gap between the insert and the wall has been neglected for the present analysis since its influence on the phenomena studied here remains very small. A sketch of the geometry is shown in Fig.1. Near the axial position $x = 0$ the insulation is interrupted between $-l \leq x \leq l$ to give welding tools free access to the bare duct wall.

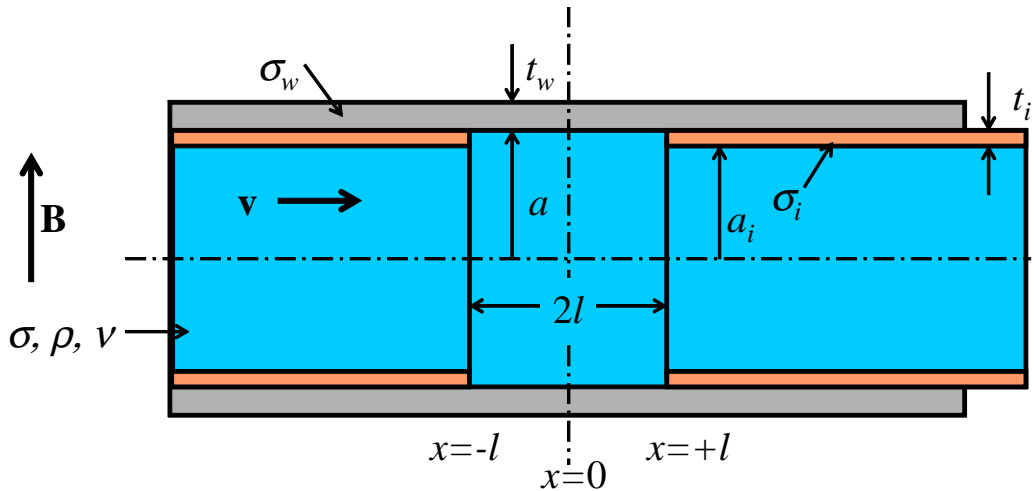


Figure 1: Sketch of the geometry used in calculations. The FCI is interrupted over a length $2l$.

2 Formulation

The flow of the liquid breeder with density ρ , electric conductivity σ and kinematic viscosity ν under the influence of a strong magnetic field is described by the non-dimensional momentum equation

$$\frac{1}{N} \left(\frac{\partial \mathbf{v}}{\partial t} + (\mathbf{v} \cdot \nabla) \mathbf{v} \right) = -\nabla p + \frac{1}{Ha^2} \nabla^2 \mathbf{v} + \mathbf{j} \times \mathbf{B}, \quad (1)$$

where \mathbf{B} , \mathbf{v} , \mathbf{j} and p stand for the magnetic field, velocity, electric current density and pressure, scaled by the reference values B_0 , u_0 , $\sigma u_0 B_0$ and $\sigma a u_0 B_0^2$, respectively. Here B_0 is a typical magnitude of the magnetic field, u_0 is the average velocity in the pipe (without insert) and a stands for the radius of the pipe (see Fig.1). The current density is determined by dimensionless Ohm's law as

$$\mathbf{j} = -\nabla \phi + \mathbf{v} \times \mathbf{B}, \quad (2)$$

where ϕ represents the electric potential, scaled by $a u_0 B_0$. Conservation of mass and charge is satisfied by

$$\nabla \cdot \mathbf{v} = 0 \text{ and } \nabla \cdot \mathbf{j} = 0. \quad (3)$$

At fluid-solid interfaces, i.e. at walls or inserts, the flow satisfies the no-slip condition, continuity of wall-normal currents and electric potential,

$$\mathbf{v} = 0, \quad j_n = j_{n,w,i} \text{ and } \phi = \phi_{w,i}. \quad (4)$$

When the fluid has direct contact with the wall, in the interval $-l < x < l$ and if the thickness t_w of electrically conducting walls is much smaller than the characteristic length scale of the problem, i.e. $t_w \ll a$, the conductance of the wall can be modelled by the so-called thin-wall condition (Walker (1981))

$$\mathbf{j} \cdot \mathbf{n} = \nabla \cdot (c \nabla_t \phi_w) \quad \text{with } c = \frac{t_w \sigma_w}{a \sigma}, \quad (5)$$

where currents entering the wall continue their paths in wall-tangential direction. Here ∇_t stands for the projection of the gradient operator tangential to the wall and c denotes the wall conductance ratio.

For the interfaces between fluid and FCI we use a different approach. Here we assume that the ceramic material is a poor electric conductor so that it is justified to neglect its conductance along the circumferential direction in comparison with the conductance of the viscous boundary layers along the interface. However, since the insert is thin, we allow an exchange of currents across the insert into the well conducting wall

$$\mathbf{j} \cdot \mathbf{n} = \frac{1}{\kappa} (\phi_w - \phi) \approx -\frac{1}{\kappa} \phi, \quad \text{where } \kappa = \frac{t_i \sigma}{a \sigma_i} \quad (6)$$

stands for the wall normal non-dimensional (contact) resistance as used in Samad (1985), Bühler and Molokov (1994). It has been conservatively assumed that the wall potential ϕ_w in (6) is negligible.

The strong magnetic field present in DCLL blankets yields non-dimensional interaction parameters and Hartmann numbers of the order of

$$N = \frac{\sigma a B^2}{\rho u_0} > 10^4 \text{ and } Ha = a B_0 \sqrt{\frac{\sigma}{\rho \nu}} \gtrsim 10^4,$$

for which inertia effects may become negligibly small in most of the fluid regions and viscous effects remain confined to very thin boundary and internal layers. In the fluid cores the flow is dominated by a balance between electromagnetic Lorentz forces and pressure forces. For such conditions asymptotic methods as applied in the present work as a first approach represent a powerful tool for flow analyses. In the inertialess and limit $N \rightarrow \infty$ and for strong magnetic fields $Ha \gg 1$ the governing equations are integrated analytically along magnetic field lines which yields a "projection" of the problem onto the duct walls where the equations for potential ϕ and pressure p are solved numerically on a 2D domain. The complete 3D flow field is reconstructed afterwards by analytical relations using the latter variables. Viscous effects are neglected in the core but taken into account by a boundary layer analysis. For details see e.g. Bühler (1995). Due to the linearity of the asymptotic problem it is possible to apply symmetry conditions at the welding location,

$$p = const = 0 \quad \text{and} \quad \frac{\partial \phi}{\partial x} = 0 \quad \text{at} \quad x = 0. \quad (7)$$

The flow at the entrance of the considered geometry is assumed to be fully developed.

3 Results

The following results have been obtained using a geometry for the fluid region as outlined in the sketch of Fig.1. In these first calculations it is assumed that the insert is perfectly insulating since this should yield conservative results considering the effects at locally bare surfaces. The conductivity of these surfaces is modelled first by a wall conductance ratio of $c = 1$, which represents a relatively high conductivity of the steel walls. In a second series of simulations the pipe wall is assumed to be thin with a conductance parameter $c = 0.1$. The Hartmann number has been set in these examples to $Ha = 1000$. This value seems actually unimportant for the case of perfectly insulating inserts since it determines primarily the fully developed pressure drop in the insulating regions but it has almost no influence on the 3D behavior at the junctions of the FCIs.

3.1 Insulating inserts and walls with $c = 1.0$

A gap of length $2l$ between FCIs has severe consequences on the local flow behavior. Electric currents induced in the insulated sections of the pipe build up a significant potential difference between the duct walls. At the locations where no insulations are present we find, due to the higher conductance of the walls, a smaller transverse potential difference. As a consequence there exists axial potential gradients that drive 3D current loops which modify substantially the local velocity profile and pressure drop. The physical behavior is sketched in Fig.2.

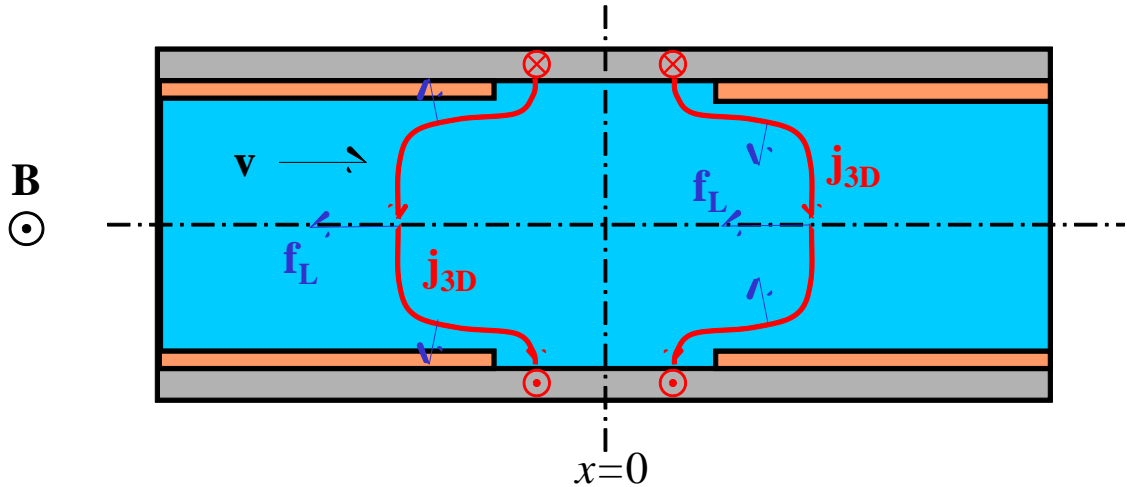


Figure 2: Principle sketch of 3D current paths and associated additional Lorentz forces.

The distribution of potential on the surface of the fluid is shown in Fig.3. For high values of Ha and poor conducting walls (inserts) the lines of constant potential represent approximate velocity streamlines. The results shown here correspond to a non-dimensional half length of the gap of $l = 0.5$. We see that the computational geometry is long enough to reach fully developed flow conditions at sufficient distance from the gap between two FCIs. Approaching the gap, the fluid is affected by the additional electric currents and the potential distribution is substantially modified already upstream of the gap.

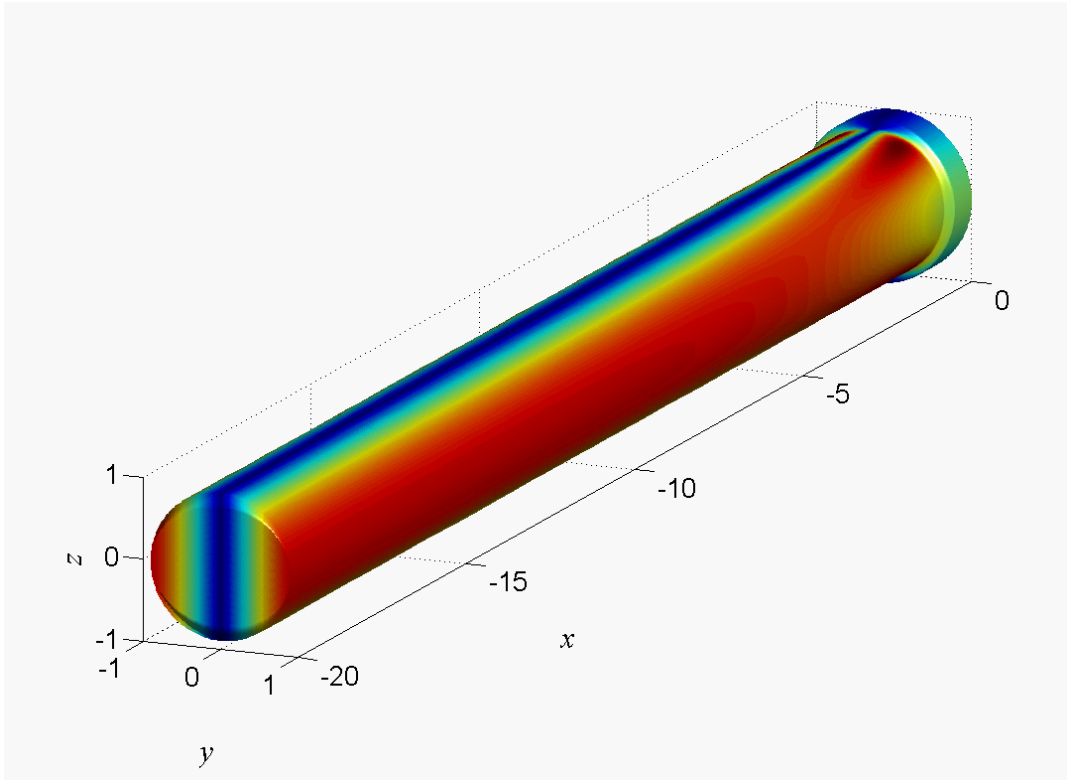


Figure 3: Colored contours of $|\phi|$ plotted on the surface of the fluid region for $c = 1$. Lines of constant color represent approximate velocity streamlines. Strong 3D effects can be observed near the end of the insulation.

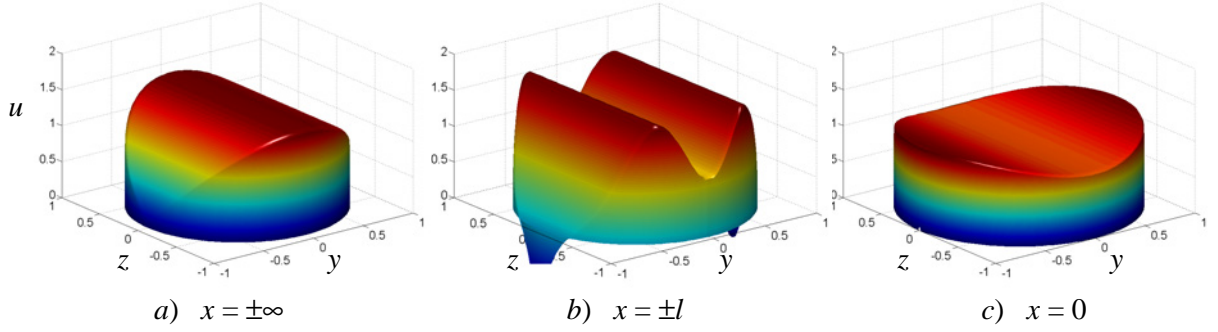


Figure 4: Velocity distributions in cross sections for three axial positions for $l = 0.5$, $c = 1$. *a)* fully developed profile as in insulating pipes for $x \rightarrow \pm\infty$, *b)* modified profile at the beginning of the gap at $x = \pm l$ and *c)* at the center of the gap at $x = 0$.

As a result the fluid redistributes along its path as shown in Fig.4. Sufficiently far from the gap ($x \rightarrow \pm\infty$) we observe a velocity profile that is typical for flows in electrically insulating pipes. We find a uniform core solution along magnetic field lines, along z , with thin Hartmann layers at walls where the magnetic field has a normal component. In transverse y direction the core velocity is not uniform but reduces towards the sides. At the beginning of the gap the flow undergoes strong modifications. The core solution is still uniform along magnetic field lines but shows two maxima and reduced values in the center. At both sides, where the magnetic field is tangent to the pipe wall, even regions with locally reversed flow may occur, as can be seen for the present flow parameters. If the gap were long enough the flow would approach in the middle of the non insulated region the fully developed profile known for conducting pipes, where the core velocity is constant. For shorter gaps some smaller deformation remains as can be seen in the Fig.4c.

Additional Lorentz forces due to 3D currents as sketched in Fig.2 modify the pressure distribution as shown in Fig.5. Far from the gap of length $2l$ we observe the fully developed non-dimensional pressure gradient of an insulating pipe flow (Shercliff (1962)), i.e.

$$\frac{\partial p}{\partial x} = -\frac{3\pi}{8Ha_i}, \quad (8)$$

where here

$$Ha_i = B_0 (a - t_i) \sqrt{\frac{\sigma}{\rho\nu}} \quad (9)$$

denotes the Hartmann number of the flow in the region where electrically insulating inserts are present. When approaching the gap between two inserts the pressure in the center (red curve) starts reducing already at some larger distance upstream as a result of the additional braking Lorentz forces caused by the 3D current loops (see Fig.2). The pressure near the sides instead increases as a result of the Lorentz forces, which push in these regions the fluid towards the wall for $x < 0$. After the flow passes the center of the gap, Lorentz forces still point upstream but now inward in order to restore the fully developed conditions of insulating MHD pipe flow as $x \rightarrow \infty$.

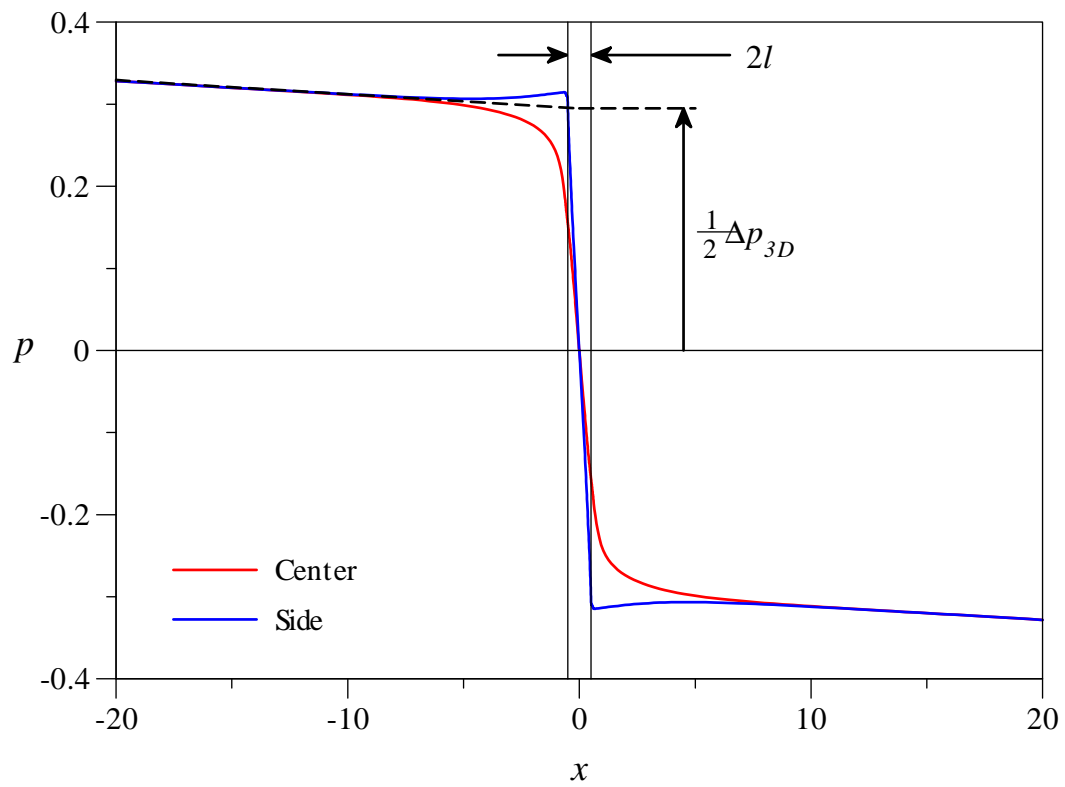


Figure 5: Nondimensional pressure distribution along the axial direction for two positions, i.e. for the center of the pipe (red) and for a location at the side (blue) for $l = 0.5$, $c = 1.0$.

As an overall result the pressure head required to drive a given flow rate increases by Δp_{3D} in comparison with an MHD flow in a perfectly insulated duct of same length. The additional pressure drop Δp_{3D} depends strongly on the length of the uninsulated section as shown later in Fig.9.

3.2 Insulating inserts and walls with $c = 0.1$

Calculations have been repeated for a series of parameters for poor conducting walls with $c = 0.1$. Results for surface potential and velocity are shown in Figs. 6 and 7. Qualitatively the solutions are similar as for the well conducting case with $c = 1$. However, 3D effects remain much smaller. This can be explained by the fact that the electric potential distribution in conducting ducts with $c \ll 1$ has similar order of magnitude as that in insulating pipes so that the axial potential gradient, which was responsible for the strong 3D effects for $c = 1$, is much weaker here. A comparison of wall potentials for poor conducting pipes shown in Fig.6 with results for higher wall conductance in Fig.3 confirms this conjecture.

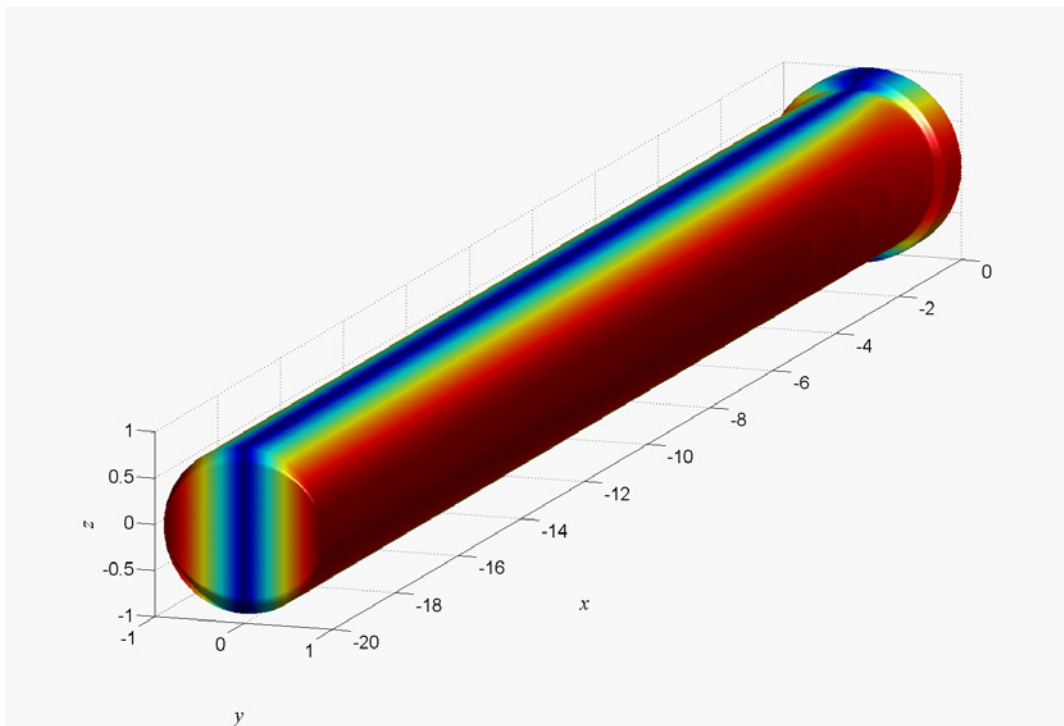


Figure 6: Colored contours of $|\phi|$ plotted on the surface of the fluid region for $c = 0.1$. Lines of constant color represent approximate velocity streamlines. 3D effects at the end of the insulation are weaker than for the case with $c = 1$ shown in Fig. 3.

Since 3D effects are less expressed for poor conductance of walls, the pressure distribution is less affected by the gap than for the case with highly conducting walls. As a result the additional pressure drop Δp_{3D} becomes much smaller as can be seen in Fig.8.

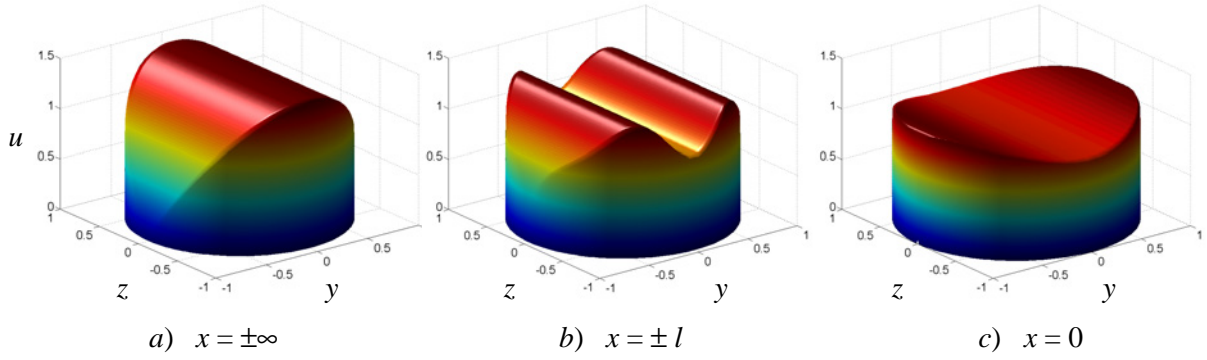


Figure 7: Velocity distributions in cross sections for three axial positions for $l = 0.5$, $c = 0.1$. *a)* fully developed profile as in insulating pipes for $x \rightarrow \pm\infty$, *b)* modified profile at $x = \pm l$ and *c)* at the center of the gap at $x = 0$.

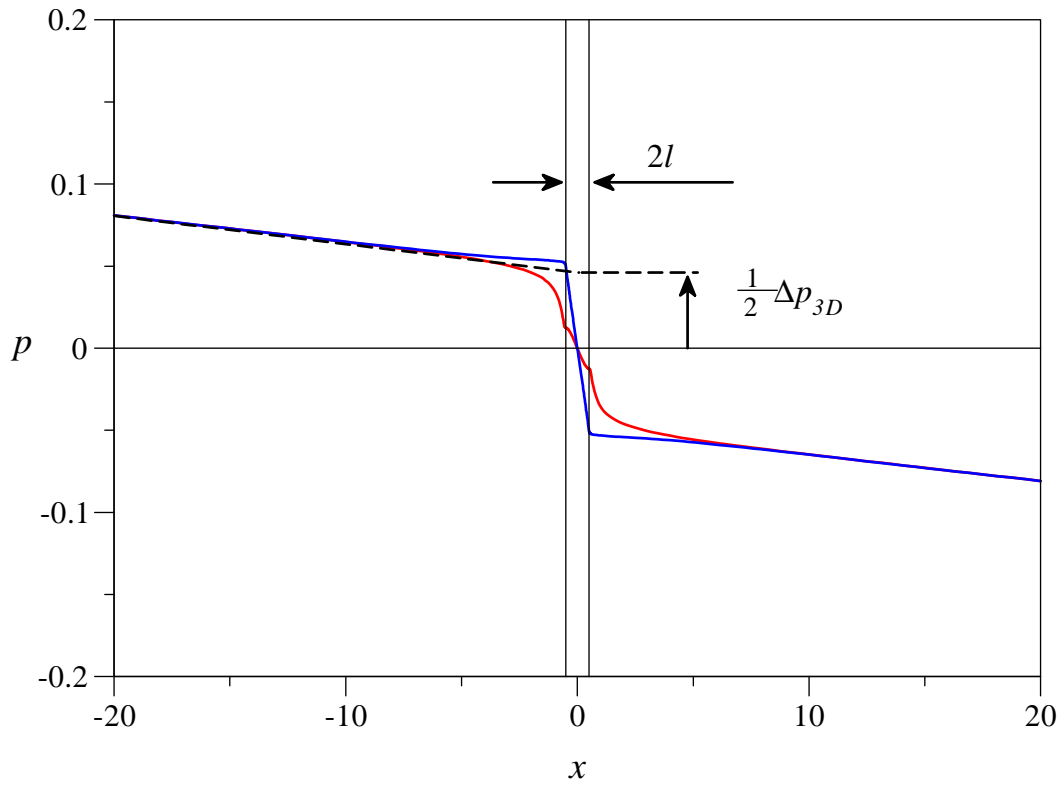


Figure 8: Pressure distribution along the axial direction for two positions, i.e. in the center of the pipe (red) and for a location at the side (blue) for $l = 0.5$, $c = 0.1$.

3.3 Pressure drop correlation

The additional pressure drop has been determined for a series of different non-insulated sections and for well and poor conducting pipes. Results are summarized in Fig.9. For both wall conductivities we find that with increasing length l , the additional pressure drop approaches apparently the asymptote

$$\Delta p_{3D} = \frac{c}{1+c} 2l. \quad (10)$$

This correlation has been confirmed for $c = 1.0$ and for $c = 0.1$. The major contribution to Δp_{3D} comes from the flow in conducting pipes, where the non-dimensional pressure gradient scales as $\partial p/\partial x = -c/(1+c)$. This pressure gradient is active along the uninsulated length $2l$ and yields Eq. (10). Due to 3D flow redistribution near $x = \pm l$ there appears another contribution which evaluates for the case of $c = 1$ to 0.0912. For insulation gaps in well-conducting pipes which are as long as a pipe radius or even longer, this fraction seems, however, unimportant. For smaller values of c such as $c = 0.1$ this correction is not required anymore as can be seen in Fig.9 where the asymptotic analysis and the correlation almost agree.

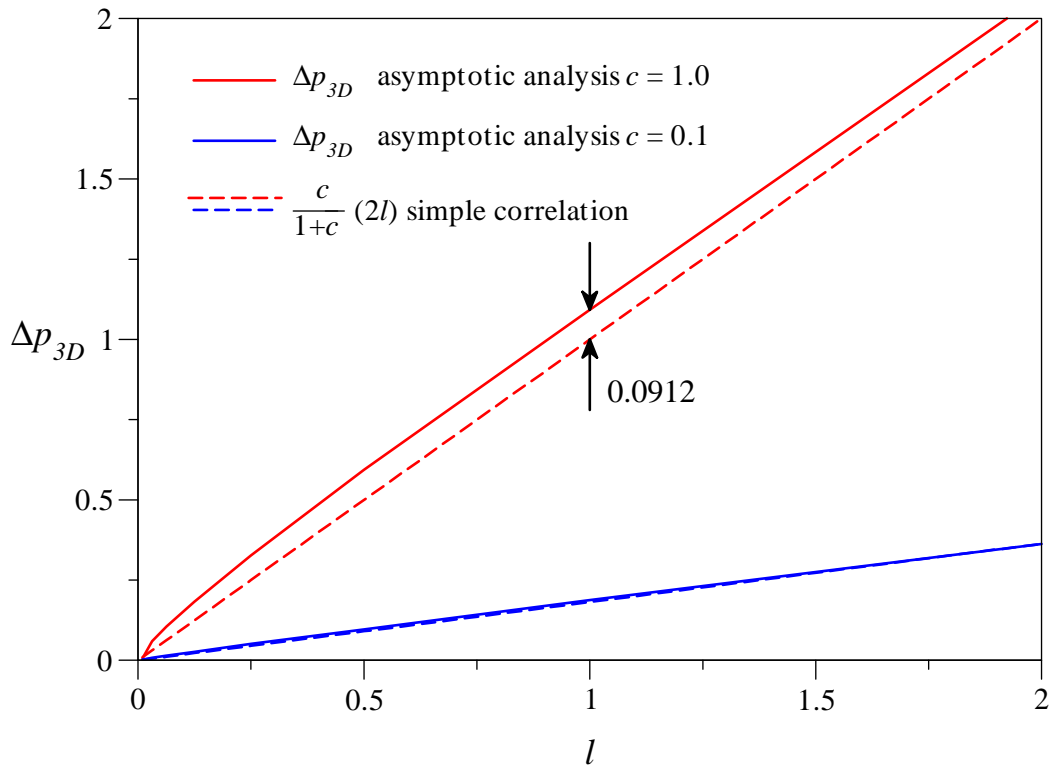


Figure 9: Additional pressure drop at junctions of insulating inserts. Comparison of results from the asymptotic analysis (solid line) with a simple correlation (dashed line).

3.4 Inserts with finite wall-normal conductivity

Up to now we assumed that the inserts were perfectly insulating, $\kappa = \frac{t_i \sigma}{a \sigma_i} = \infty$. In the following we consider cases where the wall-normal conductivity of the insulating material is varied in a wide range. This seems required since there exist no unique values in literature. The conductivity of SiC/SiC may vary between $5 \frac{1}{\Omega m} < \sigma_i < 500 \frac{1}{\Omega m}$, where the lower value is perhaps too optimistic and the higher one has been suggested under irradiation (see e.g. Giancarli, Golfier, Nishio, Raffray, Wong and Yamada (2002), Raffray, El-Guebaly, Ihli, Malang, Najmabadi, Wang and the ARIES-CS Team (2007)). In a parametric study of a fully developed MHD pipe flow we therefore investigate the pressure gradient for a wide range of κ . Calculations are performed for a fusion relevant Hartmann number of $Ha_i = 12000$ ($B = 5T$, $a = 0.1m$, $t_i = 0.01m$). Results for axial pressure gradient are shown in Fig.10. The vertical lines A and B mark the most optimistic ($\sigma_i = 5 \frac{1}{\Omega m}$) and perhaps a more realistic ($\sigma_i = 500 \frac{1}{\Omega m}$) value for κ .

For well conducting inserts, i.e. $\kappa \lesssim 1$ the non-dimensional pressure drop approaches the solution of a perfectly conducting pipe flow with $\partial p / \partial x \rightarrow 1$, while for high values of wall-normal resistance coefficient κ the solution approaches perfectly insulating conditions according to (8). This however, requires $\kappa \gg Ha$. As a result we find that $\sigma_i = 500 \frac{1}{\Omega m}$ helps already reducing the MHD pressure drop by more than two orders of magnitude in comparison to cases without insulation but this value is still almost two orders of magnitude higher than in perfectly insulating pipes.

Currents leaking into the well conducting wall have an impact on velocity profiles in MHD pipe flow as shown in Fig.11 for the four values of $\kappa = 10, 10^2, 10^3, 10^4$ as indicated in Fig.10 by the symbols (a)-(d). It can be seen that for the case *a*) we find the typical solution of MHD flows in well conducting ducts with a uniform core velocity. With increasing κ the velocity near the sides at $y = \pm 1$ starts reducing while the velocity in the center increases. For case *d*) the velocity profile corresponds practically to that in an insulating pipe (Shercliff (1962)).

Calculations have been also performed for cases with locally non-insulated duct walls. It has been found that the additional pressure drop in the region $-l < x < -l$ compared with that in a duct completely covered with an insert remains almost unchanged even if κ varies over a wide range, provided that $\kappa \gg 1$.

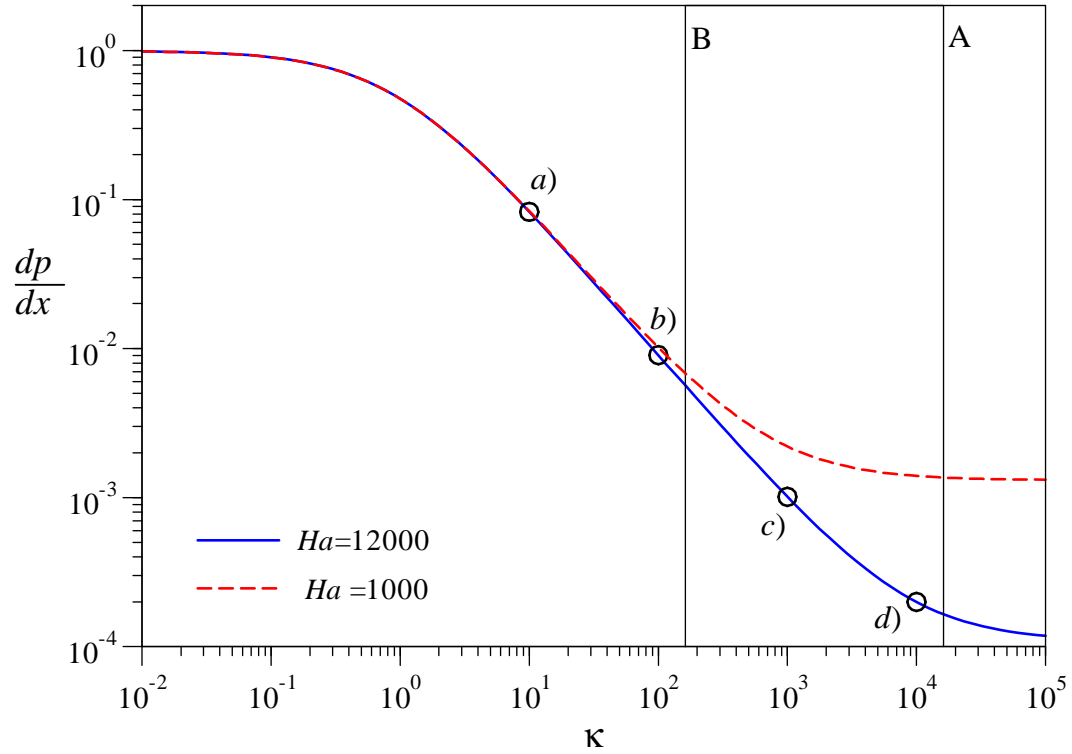


Figure 10: Nondimensional pressure gradient of a fully developed MHD flow at $Ha_i = 12000$ in a perfectly conducting pipe with a FCI of finite wall-normal conductivity given by the nondimensional resistance κ . Symbols marked with letters *a) ÷ d)* indicate the flow parameters for which velocity profiles are shown in Fig.11

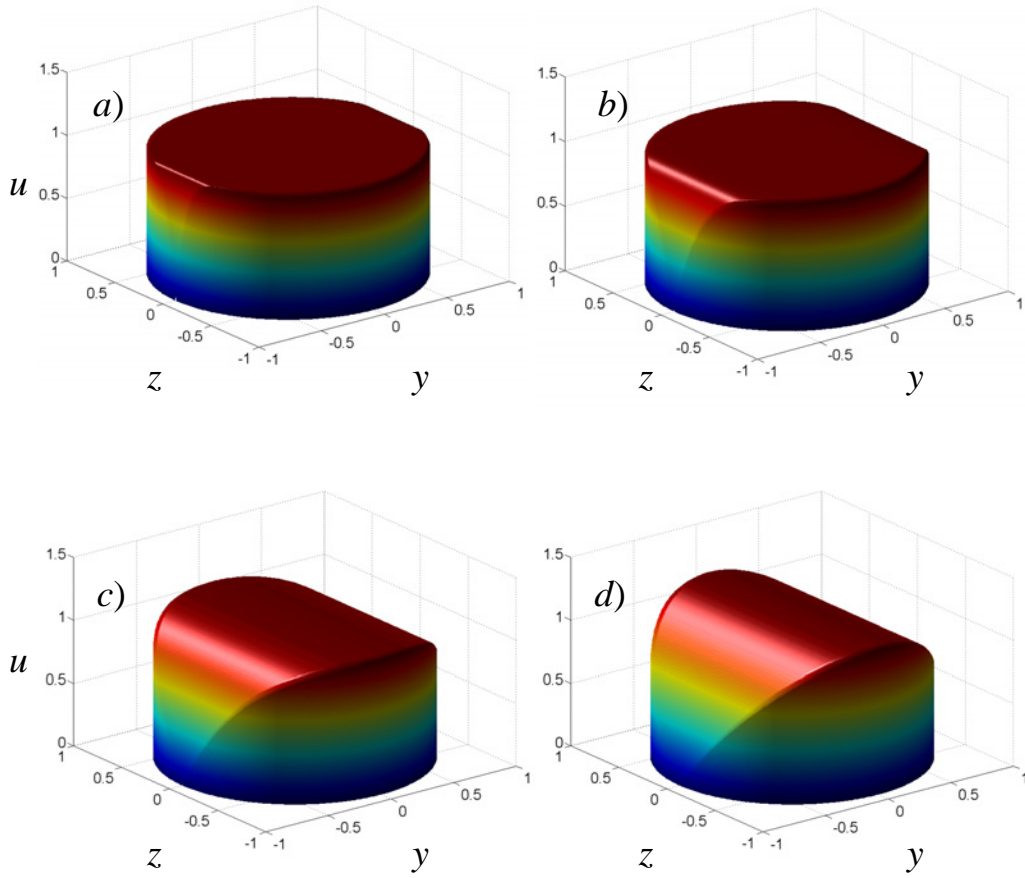


Figure 11: Velocity profiles of a fully developed MHD flow in a highly conducting pipe with FCIs of finite wall-normal conductivity for a) $\kappa = 10$, b) $\kappa = 10^2$, c) $\kappa = 10^3$, d) $\kappa = 10^4$ as indicated by the symbols in Fig. 10.

4 Conclusions

A systematic parametric analysis has been performed using asymptotic numerical methods for determination of MHD flows near gaps of insulating inserts in well conducting pipes. Such gaps could be required at several positions in fusion blankets, where cutting and rewelding by remote controlled tools is foreseen. Gaps in the insulation provide additional current paths which leads to increased current density and braking Lorentz forces. As a result the overall pressure drop increases significantly in comparison with that in a perfectly insulating pipe. The present numerical simulations suggest a simple design formula (10) which should give a conservative estimate of the additional pressure drop Δp_{3D} .

Since a specific detailed design for a DCLL module does not yet exist and velocities are unknown for the moment, we apply our results to a number of parameter cases as shown in Tab.2 and Tab.3. For the geometry we assume a pipe radius of $a = 0.1m$ and a thickness for the insert of $t_i = 0.01m$. The fluid properties have been used according to Tab.1 for PbLi at a reference temperature of $550^\circ C$ taken from Jauch, Karcher, Schulz and Haase (1986).

PbLi at $550^\circ C$		
ρ	$[kg/m^3]$	9.541×10^3
ν	$[m^2/s]$	1.07×10^{-7}
σ	$[1/\Omega m]$	7.28×10^5

Table 1: Properties of PbLi

l/a	$\Delta p_{3D} [MPa]$							
	$B [T]$	$u_0 [m/s]$	$B [T]$	$u_0 [m/s]$	$B [T]$	$u_0 [m/s]$	$B [T]$	$u_0 [m/s]$
	1	0.1	1	1	10	0.1	10	1
0.0625	0.000767		0.0076		0.0767		0.7673	
0.125	0.001331		0.0133		0.1331		1.3315	
0.25	0.002377		0.0237		0.2377		2.3770	
0.5	0.004320		0.0432		0.4320		4.3207	
1	0.007949		0.0794		0.7949		7.9490	
2	0.015115		0.1511		1.5115		15.115	

Table 2: Additional pressure drop at gaps of flow channel inserts for $c = 1$

Results displayed in Tab.2 show that at high magnetic fields $B = 10T$ as they may occur e.g. at inboard blanket modules and for coolant velocities of $u_0 = 1m/s$ a single gap of length $2l = 2 \times 0.0625a = 12.5mm$ without insulation may create already an additional pressure drop of $\Delta p_{3D} = 0.767MPa$ if walls are well conducting. This value appears already too high to be acceptable although the length of the uninsulated gap is eventually already too short for welding purposes. For smaller wall conductance parameters, e.g. for $c = 0.1$, the additional pressure drop reduces by an order of magnitude but values displayed in Tab.3 seem still quite high depending on the magnitude of the magnetic field and the mean velocity foreseen for the flow.

l/a	$\Delta p_{3D} [MPa]$							
	$B [T]$	$u_0 [m/s]$	$B [T]$	$u_0 [m/s]$	$B [T]$	$u_0 [m/s]$	$B [T]$	$u_0 [m/s]$
	1	0.1	1	1	10	0.1	10	1
0.0625	0.000107		0.00107		0.01075		0.1075	
0.125	0.000191		0.001916		0.01916		0.1916	
0.25	0.000371		0.003711		0.03711		0.3711	
0.5	0.000704		0.007048		0.07048		0.704	
1	0.001364		0.013649		0.13649		1.3649	
2	0.002641		0.026412		0.26412		2.6412	

Table 3: Additional pressure drop at gaps of flow channel inserts for $c = 0.1$

The present analysis shows clearly the need of seamless insulating inserts in the regions of strong magnetic field. Already short uninsulated gaps can create unacceptably high additional pressure drops.

Finally a few remarks should be made on the assumptions on which the present analysis is based on.

A first assumption was that currents may close in the wall only in an axial region of length $-l < x < l$. This is an ideal assumption since once currents penetrate the wall they may flow also in regions behind the insulation with much less resistance. This effect would lead to a further increase in Δp_{3D} .

On the other hand the present analysis is based on an inertialess theory. The strong modifications of the flow near the junctions of FCIs will not be free of inertia effects. There is still the possibility that a complete numerical simulation that takes into account also inertia effects may yield smaller values than those predicted in the present report. Such calculations are beyond the scope of the present work and will be performed in future.

Annex

Inventions & Know-how

The results obtained within the studies performed under this task did not yield any specific innovation or intellectual property.

References

- Bühler, L.: 1995, Magnetohydrodynamic flows in arbitrary geometries in strong, nonuniform magnetic fields, *Fusion Technology* **27**, 3–24.
- Bühler, L. and Molokov, S.: 1994, Magnetohydrodynamic flows in ducts with insulating coatings, *Magnetohydrodynamics* **30**(4), 439–447.
- Giancarli, L., Golfier, H., Nishio, S., Raffray, R., Wong, C. and Yamada, R.: 2002, Progress in blanket designs using SiCf/SiC composites, *Fusion Engineering and Design* **61-62**, 307–318.
- Jauch, U., Karcher, V., Schulz, B. and Haase, G.: 1986, Thermophysical properties in the system Li-Pb, *Technical Report KfK 4144*, Kernforschungszentrum Karlsruhe.
- Malang, S., Deckers, H., Fischer, U., John, H., Meyder, R., Norajitra, P., Reimann, J., Reiser, H. and Rust, K.: 1991, Self-cooled blanket concepts using pb-17li as liquid breeder and coolant, *Fusion Engineering and Design* **14**(3-4), 373–399.
- Norajitra, P., Bühler, L., Fischer, U., Kleefeldt, K., Malang, S., Reimann, G., Schnauder, H., Giancarli, L., Golfier, H., Poitevin, Y. and Salavy, J. F.: 2001, The EU advanced lead lithium blanket concept using SiCf/SiC flow channel inserts as electrical and thermal insulators, *Fusion Engineering and Design* **58-59**, 629–634.
- Raffray, A. R., El-Guebaly, L., Ihli, T., Malang, S., Najmabadi, F., Wang, X. and the ARIES-CS Team: 2007, Engineering challenges in designing an attractive compact stellarator power plant, *Fusion Engineering and Design* **82**, 2696–2704.
- Samad, S. A.: 1985, Effect of contact resistance on steady MHD flows through circular pipes having constant conductivity and finite wall thickness, *International Journal of Engineering Science* **23**(9), 969–974.
- Shercliff, J. A.: 1962, Magnetohydrodynamic pipe flow Part 2. High Hartmann number, *Journal of Fluid Mechanics* **13**, 513–518.
- Walker, J. S.: 1981, Magnetohydrodynamic flows in rectangular ducts with thin conducting walls, *Journal de Mécanique* **20**(1), 79–112.

